IEEE Access
Multidisciplinary | Rapid Review | Open Access Journal

Received May 14, 2019, accepted June 17, 2019, date of publication June 24, 2019, date of current version July 12, 2019.

Digital Object Identifier 10.1109/ACCESS.2019.2924592

Performance Evaluation of Variable Structure Controller Based on Sliding Mode Technique for a Grid-Connected Solar Network

HAZEM F. FESHARA[1], AMR M. IBRAHIM[2], NOHA H. EL-AMARY[3], AND SOLIMAN M. SHARAF[1]

[1]Faculty of Engineering, Helwan University, Helwan 11795, Egypt
[2]Faculty of Engineering, Ain Shams University, Cairo 11517, Egypt
[3]Arab Academy for Science, Technology and Maritime Transport, Cairo 2033, Egypt

Corresponding author: Hazem F. Feshara (feshara@gmail.com)

ABSTRACT Generating electric power from solar energy is a vastly growing technology worldwide. This paper investigates and evaluates the performance of a solar power generation system utilizing variable structure control with sliding mode for maximum power point tracking (MPPT). This controller is implemented on a buck–boost dc–dc power converter to track the maximum power point (MPP). The suggested controlled solar energy system also includes a dc-link capacitance, a voltage-source inverter, and a grid filter. Energy-based control is performed for the voltage of the dc-link capacitor. Space vector pulsewidth modulation (SVPWM) with current control in *dq* rotating frame is utilized to govern the inverter. The suggested system is simulated and subjected to various operating conditions. The results demonstrate the power captured from photovoltaic (PV) panels and delivered to the grid while tracking the MPP. For more confidence on the MPPT controller, practical experimentation is introduced using a real PV panel and power circuit with interfacing to a personal computer (PC). The proposed design is subjected to various experimental tests to ensure its validity.

INDEX TERMS DC-DC power converters, maximum power point trackers, sliding mode control, solar energy, space vector pulse width modulation, variable structure systems.

I. INTRODUCTION

Solar energy is one of the vital renewable energy resources that can provide energy to electrical networks with low environmental cost compared with traditional ways of energy production. Low proficiency and characteristics nonlinearity of PV panels, together with continuous change in radiations from sunlight and surrounding temperature make it important to acquire a Maximum Power Point tracking (MPPT) process [1]. That's why research of the MPPT control methods has been paid extensive attention by many researchers [2]–[10].

Photovoltaic (PV) energy modules are often linked to converters in order to capture the maximum available amount of power. For transferring the generated DC power to the electrical network, inverters can provide many control acts in conjunction with their main objectives such as dynamic controlling of active and reactive power and reactive current injection during faults [6]–[9].

MPPT function is the key point of any photovoltaic power processing system [10]. To track Maximum Power Point (MPP), variable structure controlled via sliding mode (shortly named Sliding Mode Control (SMC)) is employed in this work on a DC-to-DC converter. SMC is a non-linear control methodology that is convenient with this type of converters realizing both robustness and stability [11]. SMC is a highly active area of research [12]–[24]. Comparing SMC with the other MPPT techniques for PV arrays, SMC is identified by not being PV array dependent, needs no periodic tuning, has fast convergence speed, and has medium implementation complexity [25].

In this paper, a variable structure controller based on sliding mode technique for maximum power point tracking is implemented to a grid-connected photovoltaic generation system. The suggested solar energy system includes buck-boost DC-to-DC converters, DC-link capacitance, a voltage source inverter, and a grid filter. The performance of the

The associate editor coordinating the review of this manuscript and approving it for publication was Ning Sun.

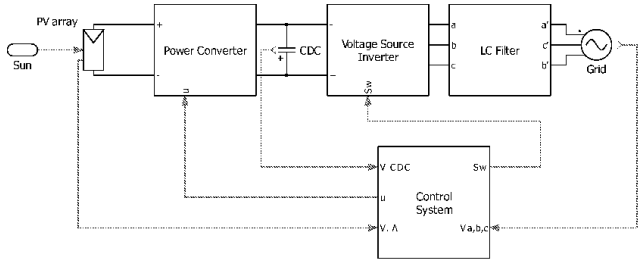

FIGURE 1. Block diagram of the solar generation system.

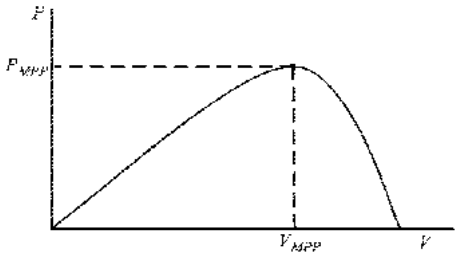

FIGURE 2. PV panels power curve.

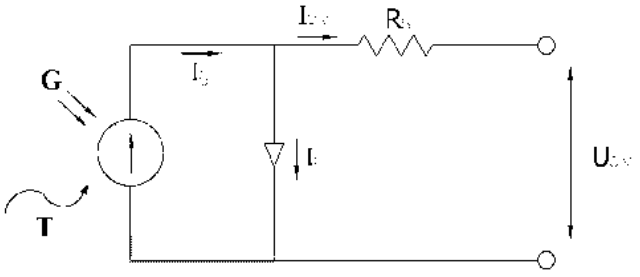

FIGURE 3. Circuit diagram of the PV panel module.

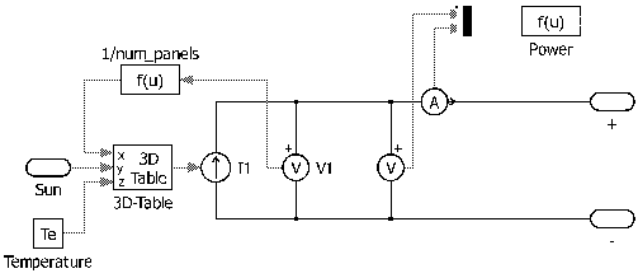

FIGURE 4. PLECS implementation of PV panels module.

suggested controller is investigated. Furthermore, Practical experiments on a real solar module interfaced to a PC are performed.

II. THE SUGGESTED SOLAR ENERGY SYSTEM

The suggested controlled solar energy system includes PV panels, DC-DC power converter, DC-link capacitor, voltage source inverter, and grid filter. Variable structure control based on SMC is utilized on the power converter for maximum power tracking. For DC-link, energy-based voltage control is utilized. For the inverter, Space Vector Pulse Width Modulation (SVPWM) with current control in *dq* rotating frame is applied to synthesize the switching signals for power transistors. Synchronization between the grid voltage and the frame of rotation is achieved via Phase Locked Loop (PLL) methodology. Block diagram of the suggested system is illustrated in Fig.1.

III. THE SUGGESTED SOLAR ENERGY SYSTEM

In this section, components of the grid-connected PV generation system are described with their parameters. This system is simulated in PLECS Standalone Simulation Platform.

A. PHOTOVOLTAIC PANELS

PV cells are electrically connected to form PV modules (panels). To construct an energy generating set, PV-panels are coordinated in arrays. Solar irradiation and cells temperature are the factors that greatly affect the generated energy form solar panels. According to these factors, each PV panel can produce a certain amount of voltage that influences the generated maximum power as illustrated in Fig.2.

A PV panel model considering temperature, circuit ohmic losses, semiconductor characteristics, and irradiation dependencies is used [26]. The losses are represented by the resistance R_s. the circuit diagram of the PV panel module is shown in Fig. 3. The current voltage equation of the model of the solar cell is given as follows:

$$I_{pv} = I_g - I_{sat}(e^{\frac{q}{AKT}(R_s I_{pv} + U_{pv})} - 1) \quad (1)$$

where

I_{sat}: PV array reverse saturation current (of the diode)
q: Electron charge
A: P-N junction ideality constant
K: Boltzmann's constant
T: PV array temperature
U_{pv}: PV array output voltage
I_g: Current produced by the incident light (it is directly proportional to the Sun irradiation G)

The studied current characteristics for PV panels are modeled in PLECS platform software utilizing 3D look-up tables [27]. The number of PV panels is chosen on the basis of the required generated power and voltage as described in [28]. The PLECS PV panels' model is shown in Fig. 4.

B. BUCK-BOOST POWER CONVERTER

A buck-boost converter is employed to transmit the energy form PV panels. The PLECS scheme of the converter is illustrated in Fig. 5. Input "u" represents the modes of switching for the converter transistor (SW). There are two modes of operation; whenever u equals one, SW is switching "on" whereas u equals zero, indicates that SW is "off".

The DC link capacitor (C_{DC}) at the converter terminals acts as the power resource to the inverter. The formula for choosing C_{DC} is as follows [29]:

$$C_{DC} = \frac{0.03E}{(1.8V_{\max})^2 - (1.4V_{\max})^2} \quad (2)$$

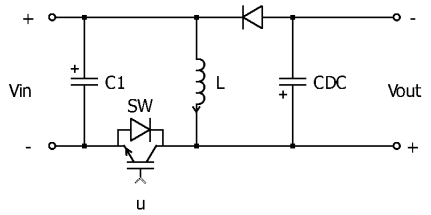

FIGURE 5. PLECS circuit diagram of buck-boost power converter.

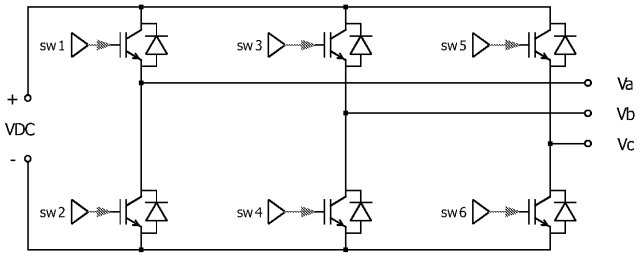

FIGURE 6. PLECS schematic diagram of VSI.

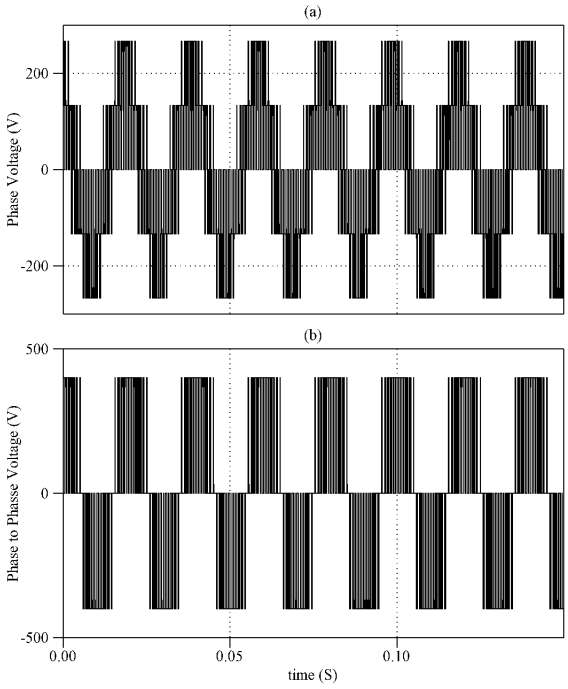

FIGURE 7. Example of inverter output: (a) Phase to neutral voltage. (b) Phase to phase voltage.

where E is the full load energy of the network and V_{max} is the peak value of network phase voltage.

C. VOLTAGE SOURCE INVERTER

The inverter is utilized to transform the DC energy stored in the DC link to the grid. Inverter output voltage is controlled via Space Vector Pulse Width Modulation technique (SVPWM). A three-phase, two-level Voltage Source Inverter (VSI) is simulated [30]. PLECS circuit diagram of VSI, with 6 IGBTs is illustrated in Fig. 6. An example for the output voltage of such inverter is illustrated in Fig. 7.

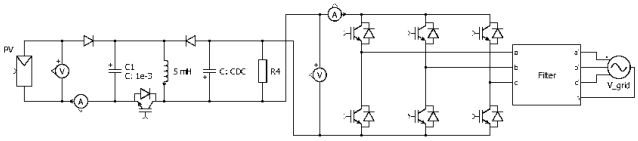

FIGURE 8. Complete PV power circuit.

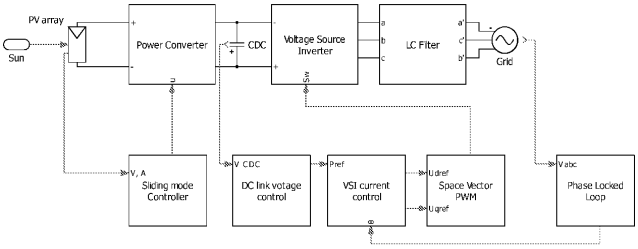

FIGURE 9. Schematic diagram of the PV generation system.

D. LC FILTER FOR GRID CONNECTION

A Low-pass *LC* filter is implemented for reducing harmonics that appear due to transistor switches operation [31], [32]. This *LC* filter is placed at the inverter's terminals with predetermined values of inductance and capacitance calculated as functions of rated power and nominal voltage [28], [32].

A complete PV power circuit diagram including the previously mentioned components is illustrated in Fig. 8.

IV. SYSTEM CONTROL

The grid-linked PV generation system utilizes several controllers; the DC-to-DC converter is controlled via sliding mode controller, another controller is employed for DC link voltage level and energy extraction, control procedures for VSI voltage is implemented, also current and power in *dq* synchronous frame are controlled. Synchronization between the grid voltages and rotating frame is accomplished through Phase Locked Loop (PLL) methodology that calculates phase angle. SVPWM is employed to deal with the switching signals for inverter transistors using calculated voltage and phase angle as references. Fig. 9 illustrates the schematic diagram of the simulated generation system with control.

A. SMC FOR MAXIMUM POWER POINT TRACKING

The output power (P_{pv}) of PV modules can be expressed as a function of modules' voltage (U_{pv}) and current (i_{pv}) as follows:

$$P_{pv} = U_{pv} i_{pv} \tag{3}$$

From the PV power curve shown in Fig. 2, two regions with different states could be distinguished: first region on the left of the maximum power point (where $dP/dV > 0$) and the second region on the right of maximum power point (where $dP/dV < 0$) [33]. Based on these two regions, converter switch

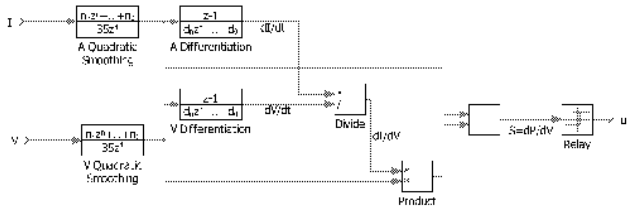

FIGURE 10. PLECS sub-system block of SMC.

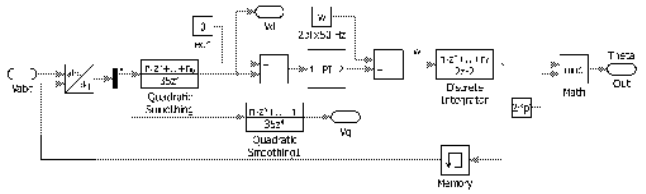

FIGURE 11. PLECS sub-system block of a PLL.

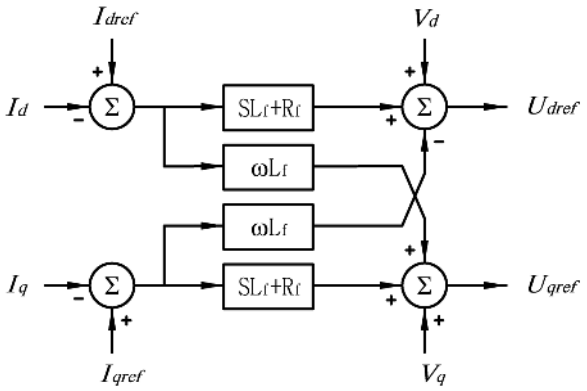

FIGURE 12. Grid current control including cross-coupling terms.

control function u is expressed as follows:

$$u = \begin{cases} 1, & S < 0 \\ 0, & S \geq 0 \end{cases} \tag{4}$$

The switching surface function S of the SMC is chosen as follows [29]:

$$S = \frac{dP_{pv}}{dU_{pv}} = \frac{di_{pv}}{dU_{pv}} U_{pv} + i_{pv} \tag{5}$$

A PLECS sub-system scheme is prepared to determine u based on PV panels measurements (voltage and current) as illustrated in Fig. 10. In order to decrease the distortion from the measurements, a 5- point quadratic smoothing function based on discrete-time domain is employed [34]. Then, the switching control and surface functions are calculated utilizing PLECS relay-block [29].

B. ENERGY-BASED DC LINK VOLTAGE CONTROL

At the terminals of the converter where DC link capacitor is set, a controlling process for the voltage of C_{DC} is accomplished in order to control the power (P_{DC}) available for the VSI taking into consideration the harmonics influence [29]. This power can be expressed as follows:

$$P_{DC} = \frac{E_{DC}}{T_H} \tag{6}$$

where T_H is the harmonic periodic time of the capacitor voltage and E_{DC} is the amount of energy available in C_{DC} which can be expressed as follows:

$$E_{DC} = \frac{1}{2} C_{DC} (V_{DC}^2 - V_{ref}^2) \tag{7}$$

where V_{DC} is the measured capacitor voltage and V_{ref} is the base voltage.

The control process of DC link capacitor voltage is achieved by selecting properly the controller gains K_{pe} and K_{ie} in order to determine the base DC-power (P_{ref}) [29]. P_{ref} can be formulated as follows:

$$P_{ref} = K_{pe}(V_{DC}^2 - V_{ref}^2) + K_{ie} \int (V_{DC}^2 - V_{ref}^2) dt \tag{8}$$

C. CURRENT CONTROL OF VOLTAGE SOURCE INVERTER

In order to submit the maximum allowable energy to the grid, with unity power factor, a controlling process for 3-phase currents of VSI has to be done [28], [35]. At the beginning, 3-phase output voltages and currents are transformed into d-components and q-components via "dq" transformation as follows [36], [37]:

$$\begin{pmatrix} V_d \\ V_q \end{pmatrix} = k \begin{pmatrix} V_a \\ V_b \\ V_c \end{pmatrix} \tag{9}$$

$$\begin{pmatrix} I_d \\ I_q \end{pmatrix} = k \begin{pmatrix} I_a \\ I_b \\ I_c \end{pmatrix} \tag{10}$$

where k is denoted as the transformation matrix. Then, voltage phase angle is extracted by employing Phase Locked Loop methodology (PLL) as illustrated in Fig. 11 [32].

In the stage when the inverter is connected to the grid, the inverter voltages in dq frame are formulated as follows [36]:

$$\begin{pmatrix} U_d \\ U_q \end{pmatrix} = L_f \frac{d}{dt} \begin{pmatrix} I_d \\ I_q \end{pmatrix} + R_f \begin{pmatrix} I_d \\ I_q \end{pmatrix} + \omega L \begin{pmatrix} -I_q \\ I_d \end{pmatrix} + \begin{pmatrix} V_d \\ V_q \end{pmatrix} \tag{11}$$

where L_f is the inductance between the inverter and the grid, R_f is the resistance between the inverter and the grid.

The following equations are used in order to determine reference voltages at inverter's terminals:

$$U_{dref} = \frac{d(I_{dref} - I_d)}{dt} L_f + (I_{dref} - I_d) R_f + V_d - \omega L_f I_q \tag{12}$$

$$U_{qref} = \frac{d(I_{qref} - I_q)}{dt} L_f + (I_{qref} - I_q) R_f + V_q + \omega L_f I_d \tag{13}$$

where I_{dref}, I_{qref} are the required currents for transferring P_{ref} to the grid [32]. Grid-filter components values (R_f & L_f) are used as controller gains that are implemented to the control scheme as shown in Fig. 12 [38].

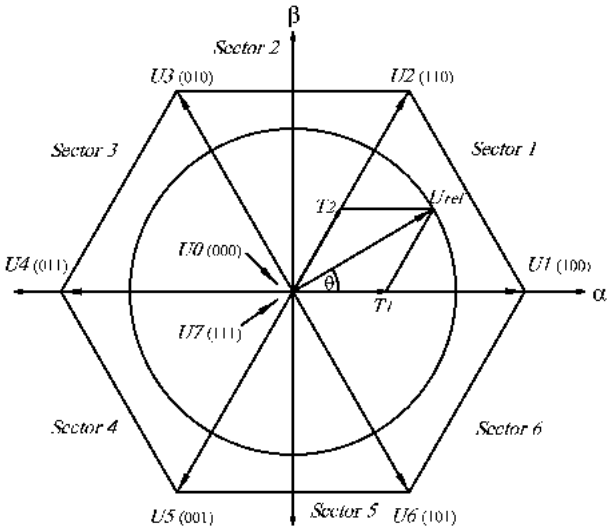

FIGURE 13. Voltage Space Vectors in SV-PWM.

This actually means the required voltage at inverter output is higher than the grid voltage with the value that causes the required current to flow from the inverter to the grid through the
filter.

D. SPACE VECTOR PULSE WIDTH MODULATION

SVPWM technique is used to produce the switching control signals that are applied to the three-phase inverter shown in Fig. 6. SVPWM as a digital modulating technique has eight switching patterns (vectors). The combination of these vectors is used to approximate the reference voltage U_{ref}. The plane of SVPWM is illustrated in Fig. 13.

This plane is divided into 6 sectors separated by 6 active vectors ($U1$ to $U6$). U_{ref} is produced via 2 adjacent non-zero vectors and 2 zero-vectors ($U0$ and $U7$). The implementation of SVPWM is explained in the following steps [28], [39]–[43]:

1) DETERMINATION OF REFERENCE VOLTAGE

Reference voltage and its reference angle are determined based on mapping the reference voltages at inverter's terminals into ($\alpha - \beta$) plane. These values are shown in the following equations:

$$U_{ref} = \sqrt{U_\alpha^2 + U_\beta^2} \tag{14}$$

$$\theta_{ref} = \tan^{-1} \frac{U_\beta}{U_\alpha} \tag{15}$$

2) DESIGNING OF SWITCHING CONFIGURATION

Three ON intervals T_a, T_b and T_c of the three upper inverter switches SW1, SW3, SW5 can be generated for each switching interval T_{sw} using the following switching time intervals; T_0, T_1 and T_2. These intervals can be demonstrated

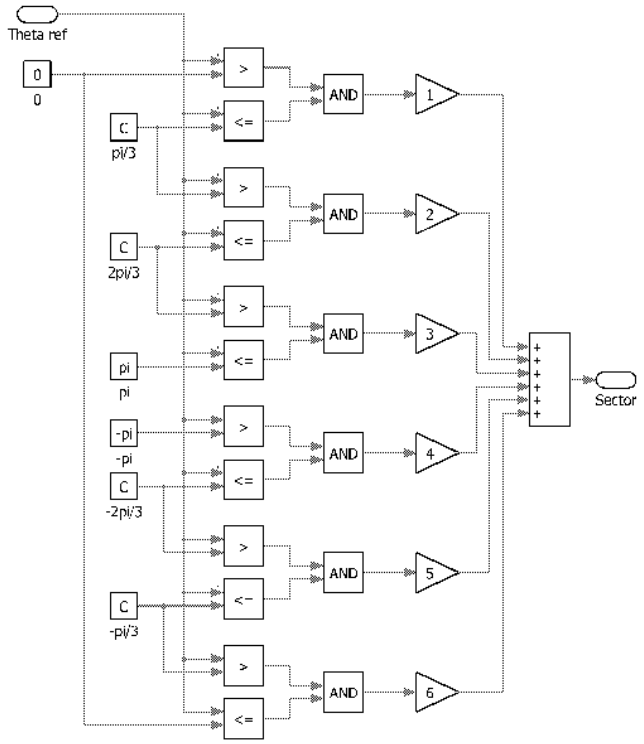

FIGURE 14. PLECS subsystem block for sector identification.

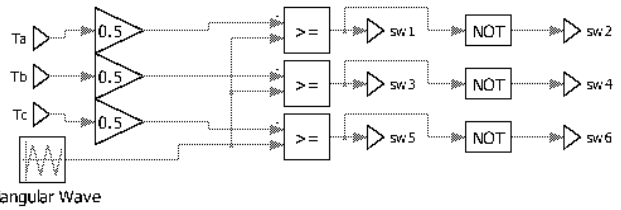

FIGURE 15. Transistors switching signals generation.

as follows:

$$T_1 = \sqrt{3} T_{sw} \frac{U_{ref}}{V_{DC}} \sin(\frac{\pi}{3} - \theta) \tag{16}$$

$$T_1 = \sqrt{3} T_{sw} \frac{U_{ref}}{V_{DC}} \sin(\theta) \tag{17}$$

$$T_0 = T_{sw} - T_1 - T_2 \tag{18}$$

where θ is the angle of reference voltage based on sector number determination which is predetermined on the PLECS platform as illustrated in Fig. 14.

Zero-vectors are used to govern the boundaries of the switching intervals. These boundaries are used to construct a table of the 6 sectors based on the switching signals. This table is executed by PLECS in order to produce the 3 ON intervals T_a, T_b and T_c.

3) PRODUCING SWITCHING SIGNALS

In order to generate the switching signals, a comparison has been made between a triangular-wave and (T_a, T_b , T_c).

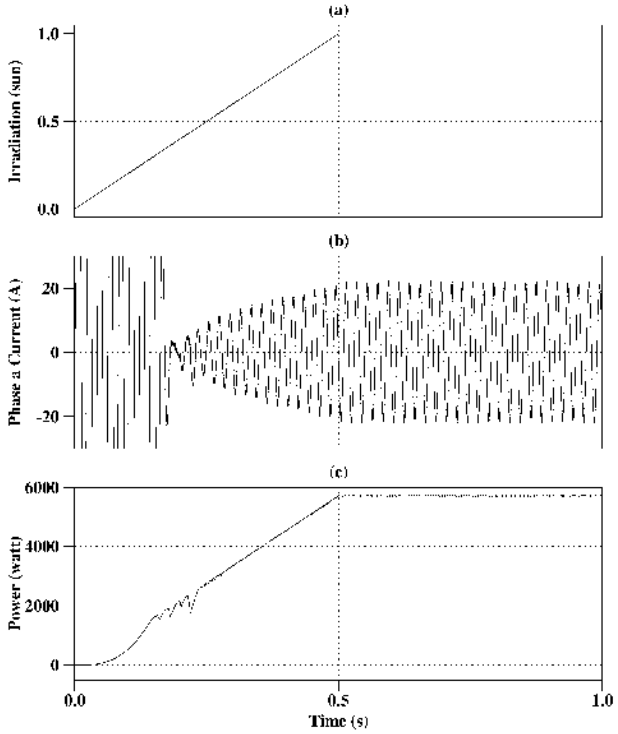

FIGURE 16. Simulation result of the PV generation system: (a) Irradiation ramp input. (b) Current at phase a. (c) PV Power.

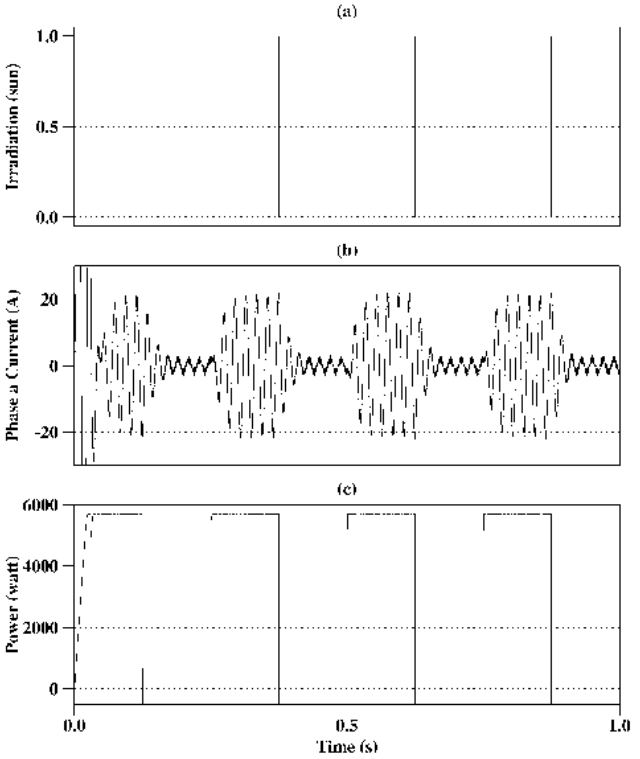

FIGURE 17. Simulation result of the PV generation system: (a) Irradiation input varying between 1 and 0. (b) Current output at phase a. (c) PV power.

TABLE 1. PV network simulating parameters.

Parameter	Description	Value
Num_panels	Number of series connected panels in the string	22
N_p	Number of PV strings connected in parallel	4
C_1	Output Capacitance connected across the PV strings	1000 μF
T_e	Operating temperature of the PV strings	25 ^{0}C
ω	Angular frequency	2Π*50 rad/sec
L	DC-DC power converter Inductance	5 mH
T	Sampling interval	0.25 ms
V_{rms}	Grid Voltage	110 V
$f_{sw} = 1/T_{sw}$	Switching frequency	4 kHz
ξc	Filter damping factor	0.5
R_f	Grid filter Resistance	1.2 Ω
T_c	Ripple period of the DC-link capacitor	0.01sec

This comparison is simulated through the design illustrated in Fig. 15.

V. SIMULATION OF PV GENERATION SYSTEM

A 6 kW network including BP365-65W modules is simulated utilizing PLECS platform to confirm the validity of the suggested control design.

A. SIMULATION PARAMETERS

Table 1 shows the parameters for the simulated network.

B. SIMULATION RESULTS

Various conditions of solar radiation are used as inputs to the PV panels. The modules signals (voltage, current and power) are monitored at the terminals of the PV panels. For 1000 W/m^2 (1 Sun) of solar radiation at 25 °C, the gross power measured form the modules is 5720W. The results are presented in Fig. 16 and Fig. 17 for two types of inputs.

Fig. 16 shows system response to a ramp irradiation input with maximum limit of 1000W/m^2. PV Power rapidly tracks irradiation level and reaches its expected rated value corresponding to 1000W/m^2. Fig. 17 shows system response to irradiation input varying from 1000 to 0 W/m2 at 4 Hz. Power at PV terminals reaches its maximum in few tens of a milli-seconds at startup then fastly tracks input power variation.

Moreover, in order to investigate the robustness of the suggested controller in tracking MPP; two systems are implemented in simulation. One of the two systems is controlled by SMC and the other one is uncontrolled. Each of the two systems is subjected to the same circumstances of operation. The results are illustrated in Fig. 18 and Fig. 19.

Fig. 18 shows the controlled and uncontrolled systems response when subjected to a step irradiation input. Fig. 19 shows controlled and uncontrolled systems response when subjected to an alternating irradiation inputs fluctuating between five irradiation levels. Power at PV terminals shows higher current and power levels achieved in case of SMC compared to uncontrolled system.

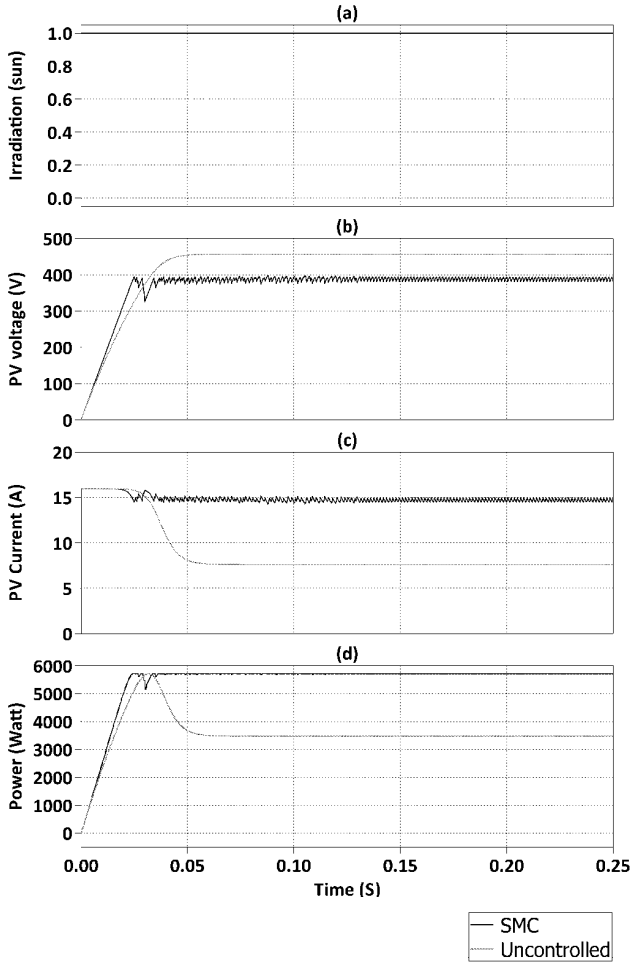

FIGURE 18. Simulation result of controlled and uncontrolled systems: (a) Irradiation input. (b) PV voltage. (c) PV current. (d) PV power.

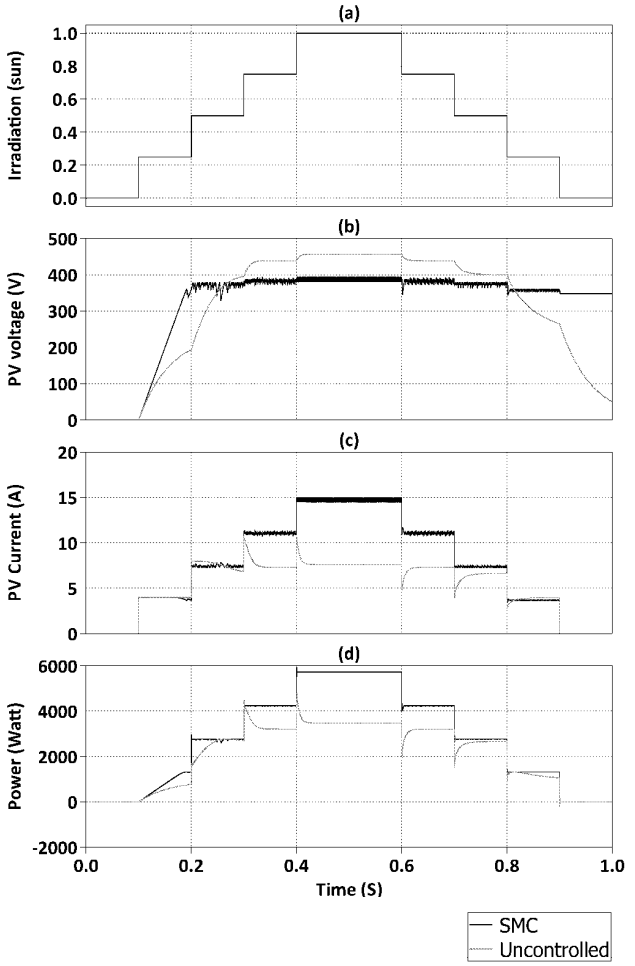

FIGURE 19. Simulation result of controlled and uncontrolled systems: (a) Irradiation input. (b) PV voltage. (c) PV current. (d) PV power.

VI. EXPERIMENTAL SETUP AND RESULTS

This section describes practical development of a photovoltaic power generation system based on interfacing an experimental prototype to a personal computer (PC). The constructed PV conversion system consists of a PV panel, a power converter, measuring circuits, controller, and load. The block diagram of the suggested PV conversion system is illustrated in Fig. 20. Also, the set of the experimental test is illustrated in Fig. 21. The controller generates base pulses for the power transistor. Software routines are developed to measure the different variables and to achieve an efficient control process. The optimum tilt angle and orientation of the PV modules for Cairo-Egypt were considered during the experiment [44].

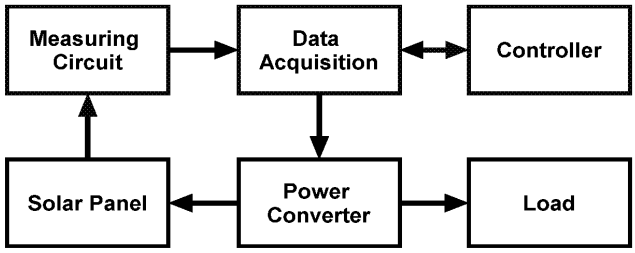

FIGURE 20. Block diagram of PV conversion system.

A. PHOTOVOLTAIC PANEL

In the experimental work, a PV-panel is connected to a DC-DC converter controlled by a SMC. The specifications of the PV-panel from its nameplate are as follows:

Module Type: AP 60 – 250
Maximum Power : 254 W
Open-circuit voltage : 37.42 VDC
Short-circuit current : 8.97 A
Voltage at maximum power : 30.01 VDC
Current at maximum power : 8.45 A
Maximum system voltage: 1000 VDC

Power is measured in standard condition (STC) of 1000 W/m^2 irradiation and cell temperature of 25 °C

B. INTERFACING MODULE

Digital control system is facilitated to operate and control the PV energy conversion system. Suitable interfacing module

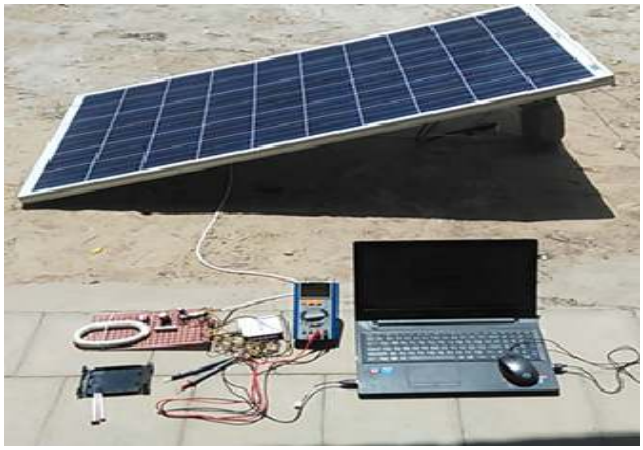

FIGURE 21. The experimental test set.

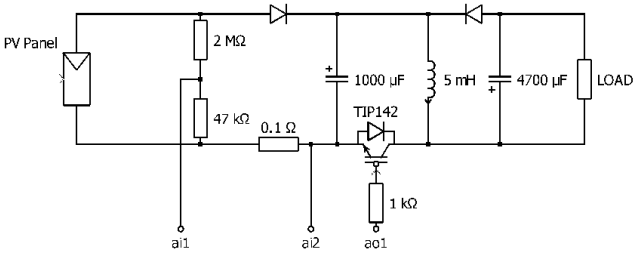

FIGURE 22. PV system circuit diagram.

is used to convert the measured signals of the PV panel to the computer. The interfacing module used is USB-6001 by National Instruments characterized by 8 analog inputs and 2 analog outputs with 14-bit resolution.

C. MEASUREMENTS CIRCUIT

A measuring module is prepared to process two analog signals; the PV panel terminals voltage and current. Complete circuit diagram of the PV module network is illustrated in Fig. 22. The measuring module includes a voltage measuring circuit based on voltage-divider concept which is designed to measure a voltage up to 50 VDC. Also, a current measuring circuit with range (0-10 A) is included.

D. SOFTWARE AND PROGRAMMING

MPPT technique based on SMC is programmed and executed using LabVIEW software and MATLAB toolbox. The MATLAB script is illustrated in a flow chart as shown in Fig. 23. The program is initialized by producing the sampling time (T) and number of total samples (n). For each sample, the voltage and current of the panel are measured. Consequently, the panel power is calculated. According to the rate of change of power to voltage (dp/dv), the switching state of the converter condition (u) is decided. At the end, PC stores the panel voltage, current, power, dp/dv and transistor switching condition.

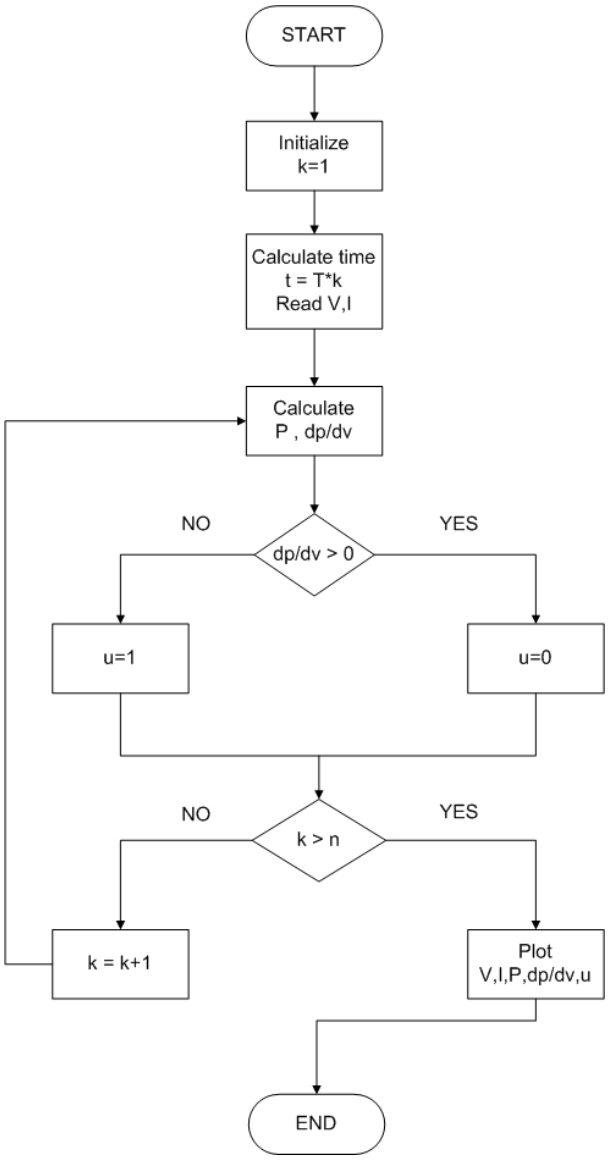

FIGURE 23. Flow chart of MATLAB script.

E. EXPERIMENTAL RESULTS OF PV ENERGY CONVERSION UNIT

Several experiments are carried out to ensure the validity and stability of the suggested controller. Experimental test results of the solar unit are plotted to investigate the effectiveness of using the sliding mode controller. The control is performed for different periods of time with a sampling interval of 25 ms. The system is interrupted by changing the irradiation using manual shading above the PV panel. System response is evaluated by observing dP/dV. Fig. 24 through Fig. 26 show the test results of the real system with SMC.

Fig. 24 shows system response of voltage, current, power, dP/dV and switching signal for fixed irradiation of 5 seconds without disturbance. Fig. 25 shows system response for irradiation of 5 seconds with 3 shading disturbances.

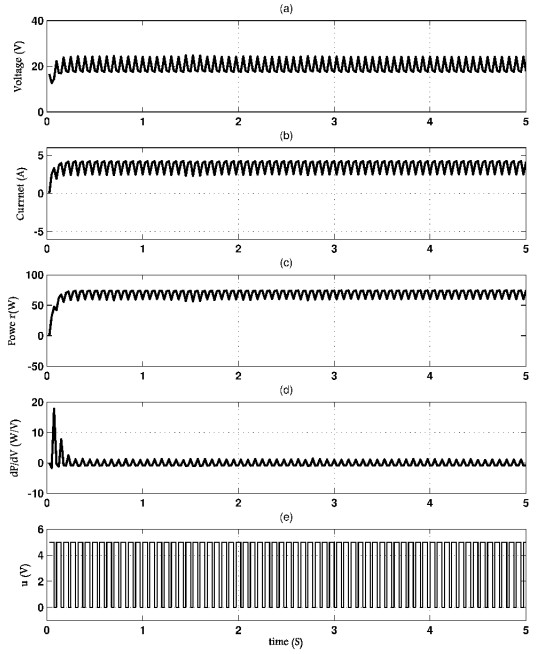

FIGURE 24. Experimental result of the PV generation system: (a) PV-panel voltage. (b) PV-panel current. (c) PV-panel power. (d) dP/dV. (e) Transistor switching signal.

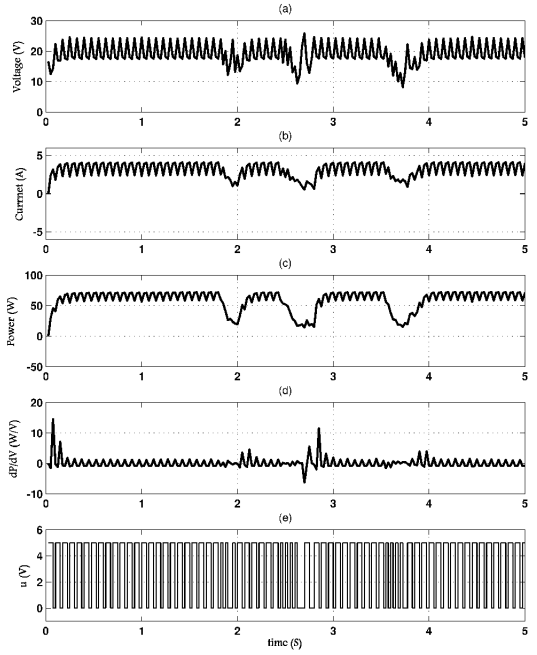

FIGURE 25. Experimental result of the PV generation system: (a) PV-panel voltage. (b) PV-panel current. (c) PV-panel power. (d) dP/dV. (e) Transistor switching signal.

Fig. 26 shows system response to irradiation for 15 seconds with one long shading disturbance.

The experimental results demonstrate that the suggested SMC always govern the system to the state where dP/dV tends to zero, and PV panel power stabilizes fast following every disturbance indicating fast convergence to MPP.

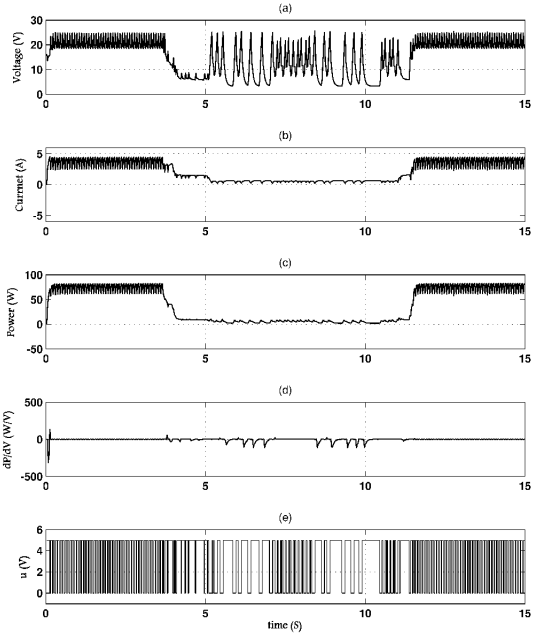

FIGURE 26. Experimental result of the PV generation system: (a) PV-panel voltage. (b) PV-panel current. (c) PV-panel power. (d) dP/dV. (e) Transistor switching signal.

VII. CONCLUSION

In this paper, a grid-connected photovoltaic generation system utilizing variable structure control with sliding mode for maximum power point tracking is investigated. The paper presents integrated multi controller architecture for energy flow in the system. The main components of the suggested system are: buck-boost DC-DC power converter, DC-link capacitor, and a voltage source inverter. Energy-based control is performed for the voltage of DC-link capacitor. Space Vector Pulse Width Modulation (SVPWM) with current control in dq-synchronous frame for power inverter is selected and executed for delivering the power to the grid. The suggested system is simulated in PLECS Simulation Platform and subjected to various inputs. Simulation results prove the robustness of the controllers. Results show that at system startup, output power takes time in order of few tens of milliseconds to stabilize. After startup, results demonstrated that the suggested design captures PV power with high tracking speed. The robustness of utilizing SMC is clear when compared with an uncontrolled system.

Furthermore, practical experiments are performed on a real solar module that interfaced to a PC. Several experiments are accomplished to ensure the validity and stability of the suggested controller. The practical results showed that the suggested SMC always drive the system towards MPP at several conditions.

It would be beneficial, in the authors' opinion; to study the following in future research: Extend practical experiments to include irradiation measurement and grid connection, Study the effect of faults, Study transient and dynamic stability requirements.

REFERENCES

[1] A. J. Mahdi, W. H. Tang, and Q. H. Wu, "Improvement of a MPPT algorithm for PV systems and its experimental validation," in *Proc. Int. Conf. Renew. Energies Power Qual.*, Granada, Spain, 2010, pp. 1–6.

[2] D. P. Hohm and M. E. Ropp, "Comparative study of maximum power point tracking algorithms," *Prog. Photovolt., Res. Appl.*, vol. 11, no. 1, pp. 47–62, Jan. 2002.

[3] N. Femia, G. Petrone, G. Spagnuolo, and M. Vitelli, "Optimization of perturb and observe maximum power point tracking method," *IEEE Trans. Power Electron.*, vol. 20, no. 4, pp. 963–973, Jul. 2005.

[4] K. H. Hussein, I. Muta, T. Hoshino, and M. Osakada, "Maximum photovoltaic power tracking: An algorithm for rapidly changing atmospheric conditions," *IEE Proc.-Gener., Transmiss. Distrib.*, vol. 142, no. 1, pp. 59–64, Jan. 1995.

[5] J. H. Lee, H. Bae, and B. H. Cho, "Advanced incremental conductance MPPT algorithm with a variable step size," in *Proc. 12th Int. Power Electron. Motion Control Conf.*, Portoroz, Slovenia, Aug./Sep. 2006, pp. 603–607.

[6] A. B. G. Bahgat, N. H. Helwa, G. E. Ahmad, and E. T. El Shenawy, "Maximum power point tracking controller for PV systems using neural networks," *Renew. Energy*, vol. 30, pp. 1257–1268, 2005.

[7] F. L. Albuquerque, A. J. Moraes, G. C. Guimaraes, S. M. R. Sanhueza, and A. R. Vaz, "Optimization of a photovoltaic system connected to electric power grid," in *Proc. IEEE/PES Transmiss. Distrib. Conf. Expo., Latin Amer.*, Sao Paulo, Brazil, Nov. 2004, pp. 645–650.

[8] F. Scapino and F. Spertino, "Load curves at DC inverter side: A useful tool to predict behavior and aid the design of grid-connected photovoltaic systems," in *Proc. IEEE Int. Symp. Ind. Electron.*, vol. 3, May 2002, pp. 981–986.

[9] S. Jain and V. Agarwal, "New current control based MPPT technique for single stage grid connected PV systems," *Energy Convers. Manage.*, vol. 48, pp. 625–644, Feb. 2007.

[10] E. Bianconi, J. Calvente, R. Giral, E. Mamarelis, G. Petrone, C. A. Ramos-Paja, G. Spagnuolo, and M. Vitelli, "A fast current-based MPPT technique employing sliding mode control," *IEEE Trans. Ind. Electron.*, vol. 60, no. 3, pp. 1168–1178, Mar. 2013.

[11] H. Guldemir, "Modeling and sliding mode control of DC-DC buck-boost converter," in *Proc. 6th Int. Adv. Technol. Symp.*, vol. 4, May 2011, pp. 475–480.

[12] J. Dannehl and F. W. Fuchs, "Discrete sliding mode current control of three-phase grid-connected PWM converters," in *Proc. 13th Eur. Conf. Power Electron. Appl.*, Sep. 2009, pp. 1–10.

[13] Y. Levron and D. Shmilovitz, "Maximum power point tracking employing sliding mode control," *IEEE Trans. Circuits Syst. I, Reg. Papers*, vol. 60, no. 3, pp. 724–732, Mar. 2013.

[14] J. Y. Hung, W. Gao, and J. C. Hung, "Variable structure control: A survey," *IEEE Trans. Ind. Electron.*, vol. 40, no. 1, pp. 2–22, Feb. 1993.

[15] V. Utkin, "Variable structure systems with sliding modes," *IEEE Trans. Autom. Control*, vol. 22, no. 2, pp. 212–222, Apr. 1977.

[16] Y. Yin, J. Liu, J. A. Sánchez, L. Wu, S. Vazquez, J. I. Leon, and L. G. Franquelo, "Observer-based adaptive sliding mode control of NPC converters: An RBF neural network approach," *IEEE Trans. Power Electron.*, vol. 34, no. 4, pp. 3831–3841, Apr. 2019.

[17] L. Khoshnevisan and X. Liu, "Fractional order predictive sliding-mode control for a class of nonlinear input-delay systems: Singular and non-singular approach," *Int. J. Syst. Sci.*, vol. 50, no. 5, pp. 1039–1051, 2019.

[18] G. Sun, L. Wu, Z. Kuang, Z. Ma, and J. Liu, "Practical tracking control of linear motor via fractional-order sliding mode," *Automatica*, vol. 94, pp. 221–235, Aug. 2018.

[19] Y. Zhao, J. Wang, F. Yan, and Y. Shen, "Adaptive sliding mode fault-tolerant control for type-2 fuzzy systems with distributed delays," *Inf. Sci.*, vol. 473, pp. 227–238, Jan. 2019.

[20] C. Du, C. Yang, F. Li, and W. Gui, "A novel asynchronous control for artificial delayed Markovian jump systems via output feedback sliding mode approach," *IEEE Trans. Syst., Man, Cybern. Syst.*, vol. 49, no. 2, pp. 364–374, Feb. 2019.

[21] J. Liu, S. Vazquez, L. Wu, A. Marque, H. Gao, and L. G. Franquelo, "Extended state observer-based sliding-mode control for three-phase power converters," *IEEE Trans. Ind. Electron.*, vol. 64, no. 1, pp. 22–31, Jan. 2017.

[22] J. Liu, L. Wu, C. Wu, W. Luo, and L. G. Franquelo, "Event-triggering dissipative control of switched stochastic systems via sliding mode," *Automatica*, vol. 103, pp. 261–273, May 2019.

[23] J. Liu, Y. Gao, X. Su, M. Wack, and L. Wu, "Disturbance-observer-based control for air management of PEM fuel cell systems via sliding mode technique," *IEEE Trans. Control Syst. Technol.*, vol. 27, no. 3, pp. 1129–1138, May 2019.

[24] G. Sun, Z. Ma, and J. Yu, "Discrete-time fractional order terminal sliding mode tracking control for linear motor," *IEEE Trans. Ind. Electron.*, vol. 65, no. 4, pp. 3386–3394, Apr. 2018.

[25] T. Esram and P. L. Chapman, "Comparison of photovoltaic array maximum power point tracking techniques," *IEEE Trans. Energy Convers.*, vol. 22, no. 2, pp. 439–449, Jun. 2007.

[26] G. Walker, "Evaluating MPPT converter topologies using a MATLAB PV model," *J. Elect. Electron. Eng.*, vol. 21, no. 1, pp. 49–56, 2001.

[27] J. Schnberger. (2009). *Modeling of a Photovoltaic String Using PLECS*. [Online]. Available: https://www.plexim.com/

[28] H. Feshara, M. Elharony, and S. Sharaf, "Design, digital control, and simulation of a grid-connected photovoltaic generation system," *Int. J. Renew. Energy Res.*, vol. 4, no. 2, pp. 484–491, 2014.

[29] K. K. Kora, "A fuzzy logic DC-Link voltage controller for three-phase DSTATCOM to compensate AC and DC loads," *Int. J. Sci. Eng. Res.*, vol. 2, no. 10, pp. 190–202, 2011.

[30] L. Malesani and P. Tomasin, "PWM current control techniques of voltage source converters-a survey," in *Proc. Int. Conf. Ind. Electron. Control Instrum.*, vol. 2, Nov. 1993, pp. 670–675.

[31] O. Mo, M. Hernes, and K. Ljøkelsøy, "Active damping of oscillations in LC-filter for line connected, current controlled, PWM voltage source converters," in *Proc. 10th Eur. Conf. Power Electron. Appl.*, Toulouse, France, 2003, pp. 49–56.

[32] H. Kim, T. Yu, and S. Choi, "Indirect current control algorithm for utility interactive inverters in distributed generation systems," *IEEE Trans. Power Electron.*, vol. 23, no. 3, pp. 1342–1347, May 2008.

[33] M. Zhang, J. Wu, and H. Zhao, "The application of slide technology in PV maximum power point tracking system," in *Proc. 5th World Congr. Intell. Control Automat.*, vol. 6, Jun. 2004, pp. 5591–5594.

[34] P. A. Gorry, "General least-squares smoothing and differentiation by the convolution (Savitzky-Golay) method," *Anal. Chem.*, vol. 62, no. 6, pp. 570–573, 1990.

[35] I.-S. Kim, "Robust maximum power point tracker using sliding mode controller for the three-phase grid-connected photovoltaic system," *Sol. Energy*, vol. 81, no. 3, pp. 405–414, 2007.

[36] Y. Yong, Y. Ruan, H.-Q. Shen, Y.-Y. Tang, and Y. Yang, "Grid-connected inverter for wind power generation system," *J. Shanghai Univ. (English Ed.)*, vol. 13, no. 1, pp. 51–56, Feb. 2009.

[37] Y. Sozer and D. A. Torrey, "Modeling and control of utility interactive inverters," *IEEE Trans. Power Electron.*, vol. 24, no. 11, pp. 2475–2483, Nov. 2009.

[38] M. Milosevic, "Decoupling control of d and q current components in three-phase voltage source inverter," ETH Zurich, Tech. Rep., 2003. [Online]. Available: https://pdfs.semanticscholar.org/d187/94558c3178d50d78df84361bbbe1056de780.pdf

[39] H. Sathishkumar and S. S. Parthasarathy, "Space vector pulse width modulation for DC-AC converter," in *Proc. 2nd Int. Conf. Sci. Technol. Eng. Manage. (ICONSTEM)*, Mar. 2016, pp. 310–314.

[40] D. Rathnakumar, J. L. Perumal, and T. Srinivasan, "A new software implementation of space vector PWM," in *Proc. IEEE SoutheastCon*, Fort Lauderdale, FL, USA, Apr. 2005, pp. 131–136.

[41] A. Abdalrahman, A. A. Zekry, and A. Alshazly, "Simulation and implementation of grid-connected inverters," *Int. J. Comput. Appl.*, vol. 60, no. 4, pp. 41–49, Dec. 2012.

[42] R. Teodorescu, M. Liserre, and P. Rodriguez, *Grid Converters for Photovoltaic and Wind Power Systems*. Hoboken, NJ, USA: Wiley, 2011.

[43] E. Hendawi, F. Khater, and A. Shaltout, "Analysis, simulation and implementation of space vector pulse width modulation inverter," in *Proc. 9th Int. Conf. Appl. Elect. Eng.*, 2010, pp. 124–131.

[44] H. M. S. Hussein, G. E. Ahmad, and H. H. EI-Ghetany, "Performance evaluation of photovoltaic modules at different tilt angles and orientations," *Energy Convers. Manage.*, vol. 45, pp. 2441–2452, Sep. 2004.

HAZEM F. FESHARA was born in Cairo, Egypt, in 1974. He received the B.Sc. degree in systems and biomedical engineering from Cairo University, Giza, Egypt, in 1997, and the M.Sc. and Ph.D. degrees in control engineering from the Electrical Power and Machines Engineering Department, Helwan University, Helwan, Egypt, in 2006 and 2017. Since 1999, he has been with ASEC Environmental Protection Company and ORBIT for Trading & Engineering Company, Cairo, where he was involved in the field of reducing industrial dust emissions and other industrial services. His M.Sc. work was awarded the Best Thesis in engineering science from Helwan University, in 2007.

AMR M. IBRAHIM was born in Egypt, in 1975. He received the B.Sc., M.Sc., and Ph.D. degrees in electrical engineering from Ain Shams University, Cairo, Egypt, in 2008, where he is currently an Assistant Professor with the Department of Electric Power and Machines. He has supervised over ten Ph.D. and M.Sc. theses in the field of electrical power system. He has taught tens of undergraduate and graduate courses in this field. He has authored or coauthored more than 40 papers. His research interests include the areas of distributed generation, renewable energy, and power system protection.

NOHA H. EL-AMARY was born in Cairo, Egypt, in 1978. She received the B.Sc., M.Sc., and Ph.D. degrees in electrical engineering from Ain Shams University, Cairo, in 2000, 2004, and 2009, respectively.

From 2004 to 2009, she was an Associate Lecturer with the Arab Academy for Science, Technology, and Maritime Transport (AASTMT), Cairo. She was an Assistant Professor with AASTMT, from 2009 to 2014. She was an Associate Professor with AASTMT, from 2014 to 2018. She has been a Professor with AASTMT, since 2018. Her research interests include artificial intelligence (AI) techniques in electrical power system stability study, analysis, measurement, and control, smart grids, and renewable energy in power systems and maritime applications.

SOLIMAN M. SHARAF was born in Minofia, Egypt, in 1949. He received the B.Sc. degree in electrical power and machine engineering from the College of Engineering and Technology, Helwan University, Cairo, Egypt, in 1972, the M.Sc. degree in power electronics engineering from Helwan University, in 1979, and the Ph.D. degree from the Queen's University of Belfast, U.K., in 1985, cooperated with Helwan University. In 1985, 1990, and 1998, he joined the Faculty of Engineering, Helwan University, as a Lecturer, an Associate Professor, and a Professor, respectively. From 2006 to 2009, he was the Head of the Electrical Power and Machines Engineering Department, Faculty of Engineering, Helwan University. From 2013 to 2014, he was the Dean of the Higher Institute of Engineering, Bilbis–Sharkiah. Since 2015, he has been a Professor and the Head of the Energy and Renewable Energy Department, Faculty of Engineering and Technology, Egyptian Chinese University, Cairo. His research interests include the control of electrical power, electrical machine engineering, renewable energy systems, wind energy, solar energy, and hybrid wind–solar systems.